Lagrangian Observations of the Deep Western Boundary Current in the North Atlantic Ocean. Part I: Large-Scale Pathways and Spreading Rates*

AMY S. BOWER AND HEATHER D. HUNT

Woods Hole Oceanographic Institution, Woods Hole, Massachusetts

(Manuscript received 10 September 1998, in final form 24 March 1999)

ABSTRACT

Twenty-six RAFOS floats were deployed in the deep western boundary current (DWBC) of the North Atlantic Ocean between the Grand Banks and Cape Hatteras in 1994–95 and tracked acoustically for up to two years. Half of the floats were launched in the upper chlorofluorocarbon (CFC) maximum associated with upper Labrador Sea Water (~800 m), and the other half near the deep CFC maximum that identifies the overflow water from the Nordic seas (~3000 m). The float observations reveal the large-scale pathways of these recently ventilated water masses in the subtropics. The shallow float tracks show directly that upper Labrador Sea Water is diverted away from the western boundary and into the interior at the location where the DWBC encounters the Gulf Stream near 36°N (the ''crossover region''), consistent with previous hydrographic studies. East of the crossover region, only one upper Labrador Sea Water float out of seven (~15%) ''permanently'' crossed to the south side of the stream in two years, caught in a cold core ring formation event. The other shallow floats recirculated north of the Gulf Stream, apparently confined by the mean potential vorticity gradient aligned with the stream. The deep floats closely followed the topography to the crossover region, then revealed a bifurcation in fluid parcel pathways. One branch continues equatorward along the western boundary, and the other turns first eastward along the Gulf Stream path, then southward. The deep float pathways, including the bifurcation in the crossover region, can be explained in terms of the deep potential vorticity distribution. Comparison of the float results with results from recent modeling studies suggests that the deep flow is strongly influenced by both the depth of the main pycnocline and bottom depth. The effective spreading rates of upper Labrador Sea Water and overflow water estimated directly from the float data, southward at 0.6 ± 0.2 cm s^{-1} and 1.4 ± 0.4 cm s^{-1}, respectively, agree well with tracer-derived spreading rates. Mean velocities in the DWBC, equatorward at 2–4 cm s^{-1} (upper Labrador Sea Water) and 4–5 cm s^{-1} (overflow water), are consistent with other in situ measurements. One deep float drifted almost 4000 km along the western boundary in two years, revealing a ''fast track'' for the spreading of overflow water in the DWBC. These observations emphasize the importance of the crossover region in the spreading and mixing of recently ventilated water masses, addressed in Part II of this study.

1. Introduction

The deep western boundary current (DWBC) in the North Atlantic Ocean is a major branch of the thermohaline circulation, and an important component in the global heat balance. It transports recently ventilated cold water masses from the northern North Atlantic toward the equatorial region along the western boundary. The existence of the DWBC was first predicted on theoretical grounds by Stommel and Arons (Stommel 1957, 1958; Stommel and Arons 1960a,b) and confirmed experimentally by Swallow and Worthington (1961) using neutrally buoyant floats.

Over the past several decades, our view of the DWBC's structure has been continually refined based on new observations. We now recognize that four separate water masses of northern origin, which together make up North Atlantic Deep Water (NADW), are transported by the DWBC in the depth range 700–4000 m. Iceland–Scotland Overflow Water and Denmark Strait Overflow Water (DSOW) make up the two deepest water masses (2500–4000 m, 2°–3°C). We will refer to these two water masses collectively as overflow water (OW). Classical Labrador Sea Water (LSW) lies above the overflow water masses in the depth range 1500–2500 m and has temperatures 3°–4°C. Upper Labrador Sea Water (ULSW), believed to form along the western boundary of the Labrador Sea, makes up the lightest component of NADW and is found in the depth range 700–1500 m with temperatures 4°–6°C (Pickart et al. 1997). Each water mass is distinguishable based on its

* WHOI Contribution Number 9805.

Corresponding author address: Dr. Amy S. Bower, Department of Physical Oceanography, Woods Hole Oceanographic Institution, Woods Hole, MA 02543.
E-mail: abower@whoi.edu

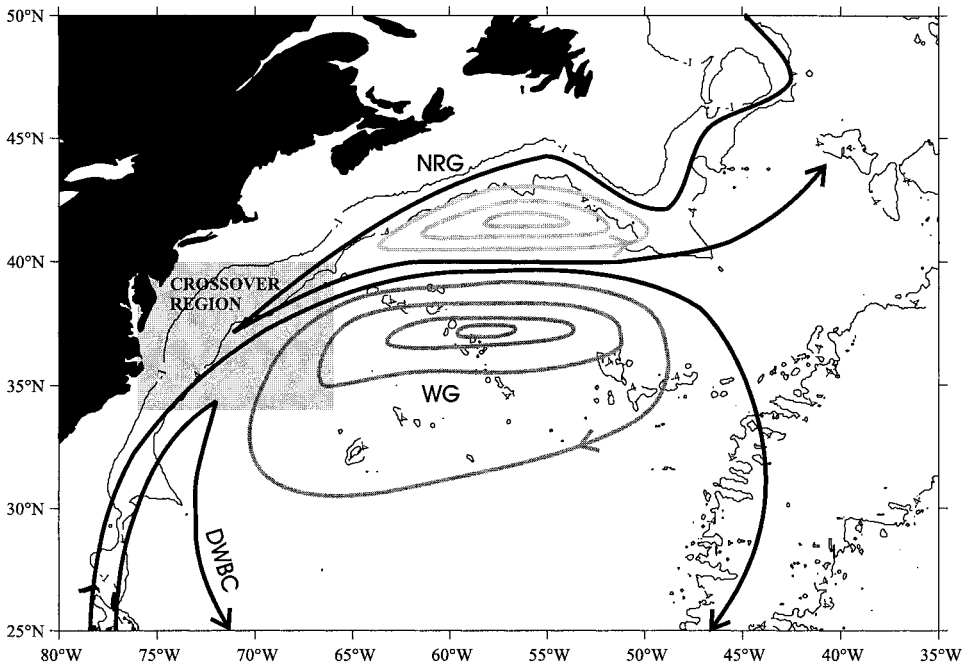

FIG. 1. Schematic diagram of the vertically integrated transport in the western North Atlantic after Hogg (1992). NRG: northern recirculation gyre, WG: Worthington gyre, DWBC: deep western boundary current. The NRG circulates cyclonically, and the WG anticyclonically. The 1-km and 4-km bathymetric contours are also shown.

characteristic water properties. Both ULSW and OW are usually identifiable as maxima in the anthropogenic tracers chlorofluorocarbon (CFC) and tritium, with DSOW contributing the most to the deep CFC core (Smethie 1993; Fine 1995). LSW is typically identified by its high dissolved oxygen content and low potential vorticity (Talley and McCartney 1982), although an increase in convective activity in the Labrador Sea in the late 1980s/early 1990s has resulted in increased levels of CFCs in this water mass (Smethie et al. 2000; Molinari et al. 1998). Tracer concentrations generally decrease seaward from, and southward along, the western boundary, consistent with an advective pathway from high latitudes along the continental slope (Doney and Jenkins 1994; Fine 1995).

A major refinement of the Stommel–Arons paradigm for the abyssal circulation has resulted from the discovery of deep recirculation gyres adjacent to the western boundary. These features have been identified in the Newfoundland Basin, north and south of the Gulf Stream extension (the northern recirculation and Worthington gyres, respectively), east of the Bahamas, and in the Guiana Basin [see Schmitz and McCartney (1993) for a review]. They can result in locally increased equatorward transport along the western boundary (see, e.g., Lee et al. 1996; Hogg 1992) and locally enhanced ventilation of the ocean interior due to mixing between the DWBC and the recirculation gyre (Olson et al. 1986; Pickart et al. 1989; Smethie 1993; Doney and Jenkins 1994; Rhein 1994). It is now well recognized that these recirculation gyres account for some of the difference between tracer-derived estimates of advective rates in the DWBC and direct velocity observations (see, e.g., Fine 1995). Tracer-derived velocities are usually in the range 1–2 cm s^{-1} (Doney and Jenkins 1994), compared to mean velocities from current meter measurements in the range 5–10 cm s^{-1} (Hogg et al. 1986; Pickart and Watts 1990; Watts 1991).

The location where the DWBC crosses under the Gulf Stream, near 36°N, is an important region of interaction between the DWBC and the ocean interior. The Gulf Stream is flowing across the slope into the deep ocean, and the western limbs of the northern recirculation gyre and the Worthington gyre are converging and turning eastward to create the deep expression of the Gulf Stream, Fig. 1 (Hogg 1992). The DWBC passes under the Gulf Stream west of the recirculation gyres and enters the subtropical regime. Pickart and Smethie (1993, hereafter PS93) conducted a detailed synoptic hydrographic and tracer survey of the crossover region and found that, except for a very narrow band of ULSW right against the slope that crossed directly under the Gulf Stream, most of the ULSW transported by the DWBC was diverted offshore at the crossover and entrained along the northern edge of the Gulf Stream. In contrast, most of the OW followed the topography more closely, crossed under the Gulf Stream, and continued

equatorward. Only the offshoremost edge of OW appeared to recirculate into the interior.

With so much of the ULSW diverted offshore in the crossover region, a natural question is how does the CFC associated with this water mass reach the subtropics and Tropics, where it has been observed against the western boundary and along the equator (Weiss et al. 1985; Fine and Molinari 1988). One explanation is that, after being deflected offshore at the crossover, ULSW is entrained from the Gulf Stream into the Worthington gyre, and returns to the western boundary south of the crossover (Smethie et al. 2000). This explanation is based on the observations of PS93 and Johns et al. (1997), who found an inflow of moderately high-CFC water into the DWBC south of Cape Hatteras. Smethie (1993) speculated that the entrainment of ULSW into the Worthington gyre occurs via the formation and dissipation of cold core rings, and PS93 suggested that strong eddy mixing right in the crossover region could result in the flux of CFCs southward across the Gulf Stream.

Some of these observations are consistent with the results of Spall (1996), who investigated the mean pathways of ULSW and OW using a three-layer regional primitive equation model. The Gulf Stream was represented in the upper layer of the model, and the DWBC in two lower layers. Like the observations of PS93, the mean flow of the upper DWBC layer (representing ULSW) showed a significant pathway deflected away from the western boundary and into the interior along the mean path of the model Gulf Stream. This flow pathway turned southward in the interior as part of the Worthington gyre and eventually returned to the western boundary south of the crossover and continued equatorward. In the lower DWBC layer (representing OW), the mean flow closely followed the topography and continued southward without being diverted significantly into the interior.

The study of PS93 significantly improved the description of the pathways of the DWBC in the crossover region, but the large-scale spreading pathways of DWBC water masses in the subtropical North Atlantic have been inferred from water property distributions and not directly observed. In the present study, we attempt to clarify the spreading pathways and rates of ULSW and OW with new Lagrangian observations obtained between the Grand Banks of Newfoundland and 20°N. These data were collected as part of a collaborative study of the DWBC using hydrographic, tracer, and float observations with R. Pickart (WHOI) and W. Smethie (LDEO), called BOUNCE (Boundary Current Experiment). The main objectives of the Lagrangian component of this investigation were to 1) directly observe long-term fluid parcel trajectories in the DWBC, including the crossover region; 2) estimate the mean equatorward speed of fluid parcels in the DWBC; and 3) investigate the kinematics and dynamics of the DWBC in the crossover region from a Lagrangian viewpoint. The first two objectives are the focus of Part I of this study, and the third objective is addressed in Part II (Bower and Hunt 2000). Future work will discuss the combined analysis of the float, hydrographic, and tracer measurements. This study complements a similar investigation of fluid parcel pathways in the DWBC south of the crossover region (Leaman and Vertes 1996). In the next section, the float dataset is described. Section 3 contains the results, which include a description of the pathways of fluid parcels in the DWBC and estimates of spreading rates of recently ventilated water masses. In section 4, we discuss the float observations in terms of previous observational and modeling results. The main findings are summarized in section 5.

2. Data

a. Float description and deployment strategy

A total of 30 Range and Fixing of Sound (RAFOS) floats were deployed in the DWBC between the Grand Banks and Cape Hatteras during two hydrographic survey cruises separated by 6 months (Fig. 2). Twenty-four floats were released on the first cruise in November–December 1994 from the R/V *Endeavor* (EN257, BOUNCE I), and six were launched on a second cruise in May–June 1995 from the R/V *Oceanus* (OC269, BOUNCE II). Half of the floats, referred to hereafter as ''shallow'' floats, were designed to be isopycnal and were ballasted for the $\sigma_t = 27.73$ density surface. This surface, which is at about 800 dbar north of the Gulf Stream, is near the center of the CFC maximum associated with ULSW (PS93; Pickart et al. 1997). The other half, referred to as ''deep'' floats, were isobaric floats, ballasted for 3000 dbar. This is near the deep CFC maximum associated with OW. All the floats were programmed to collect acoustic tracking data from moored sound sources, as well as pressure and temperature measurements, once daily for two years. At the end of its mission, each float dropped a ballast weight and returned to the sea surface, where it transmitted its data to the ARGOS satellites. Through Service ARGOS, the data were transmitted to a ground station. The data were then transferred to a global positioning center and on to WHOI via the Internet. See Rossby et al. (1986) for a more detailed description of the RAFOS system.

The shallow floats were designed to be isopycnal floats so that they could more accurately follow the horizontal and vertical pathways of fluid parcels, especially in the crossover region where isopycnal surfaces slope steeply across the Gulf Stream. The method of Rossby et al. (1985) was used to render the floats isopycnal, which involves attaching a spring-backed piston mechanism (''compressee'') to the float. The spring constant and piston diameter are chosen to give the entire float package the same compressibility as seawater.

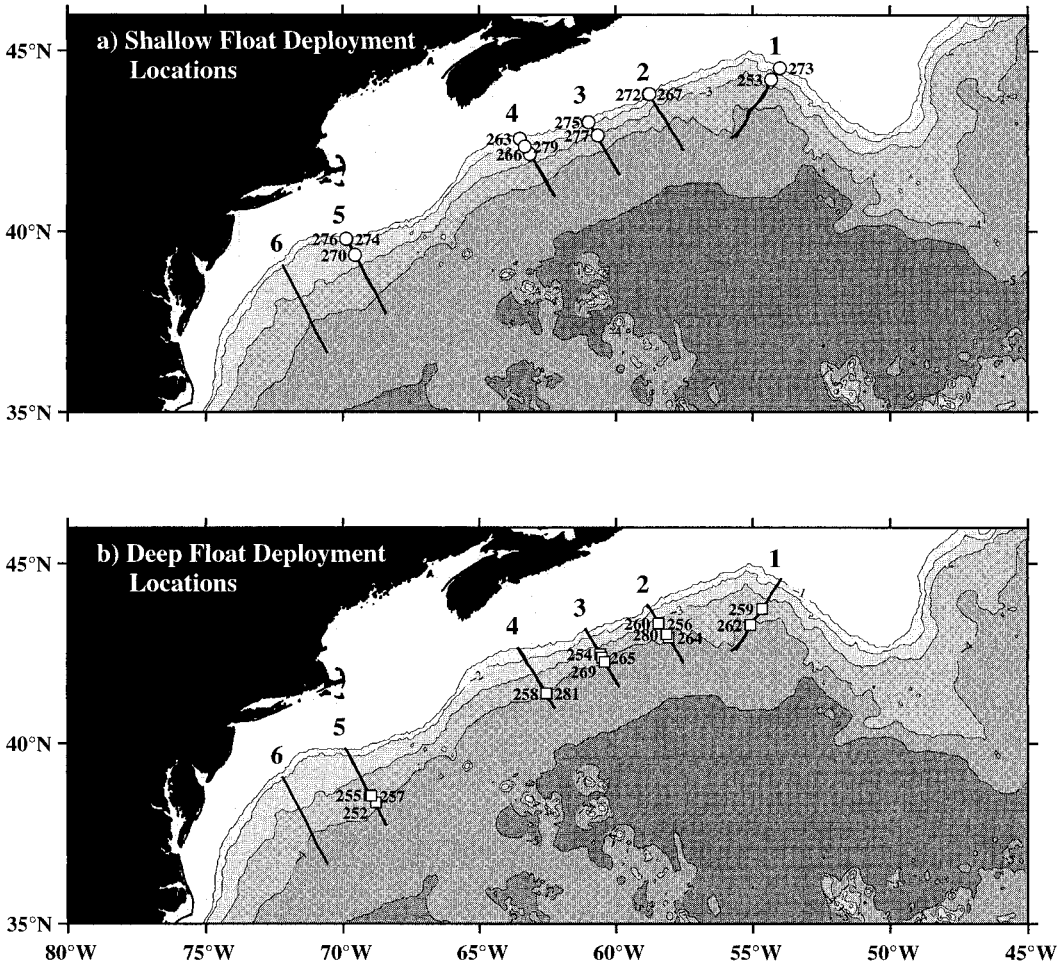

FIG. 2. Charts showing deployment sites of (a) shallow floats, deployed in the upper CFC maximum of the DWBC [~800 m depth, upper Labrador Sea Water (ULSW)], and (b) deep floats, deployed near the deep CFC maximum [~3000 m depth, overflow water (OW)] along BOUNCE CTD sections. Only the 26 floats that transmitted data are included here and in subsequent figures. Almost all of the floats were launched on the first BOUNCE cruise in Nov–Dec 1994. CTD sections 1–5 were occupied on both BOUNCE cruises, while section 6 was occupied only during BOUNCE II. Bathymetry is shaded in 1-km intervals. Most of the shallow floats were launched between the 1500 and 3000 m isobaths, and most of the deep floats between the 3500 and 4000 m isobaths.

Since the shallow floats were to be launched at the base of the main pycnocline, where the potential density gradient is relatively weak, the compressees were designed conservatively to be slightly more stiff than seawater (a float with exactly the same compressibility as seawater in a vertically homogeneous water column would be neutrally stable). Compressibilities of the shallow floats were 85%–90% of seawater compressibility at the target pressure, temperature, and salinity. The deep floats could not be made isopycnal due to the very low stratification and extreme hydrostatic pressures in the deep ocean.

Twenty-six of the 30 floats thus launched surfaced and returned data, 12 shallow and 14 deep. Figure 2 shows where they were released, and Table 1 lists the launch, surface, initial temperature and pressure, and mission information for each float. The CFC samples taken during the cruises could not be analyzed quickly enough to tailor the float launch positions to the real-time CFC distribution, so a deployment strategy based on previous observations and ''upstream'' CFC observations (as they became available during the cruise) was adopted. Along each CTD section that was seeded with floats, one shallow float was launched where the section crossed the 1500-m isobath and one or two more shallow floats were launched 25–50 km offshore to document any cross-slope dependence of float behavior (Fig. 2a). This ensured that the floats were at least several hundred meters above the seafloor. One deep float was launched where the section crossed the 3500-m isobath. The deep CFC maximum is usually found near this isobath. On most sections, one or two more deep floats were

TABLE 1. Float launch and surface information. The status code indicates how the float mission ended: normally (00) or prematurely due to low battery voltage (66), overpressure (80), or lost ballast weight (83). For float b253, the status code is unknown and assumed normal (00) because the float completed full mission length of 730 days.

	Launch			Surface						
Float	Date (yymmdd)	Latitude (°N)	Longitude (°W)	Date (yymmdd)	Latitude (°N)	Longitude (°W)	Mission length	Status code	Initial *P* (dbar)	Initial *T* (°C)
					Shallow floats					
b253	941114	44.203	54.329	961113	40.544	66.352	729	00?	939.1	3.94
b263	941122	42.560	63.501	960427	39.300	67.020	522	83	848.0	4.41
b266	941122	42.136	63.146	961117	35.086	67.802	726	00	879.5	4.55
b267	941117	43.802	58.796	961115	39.609	62.678	729	00	942.0	4.17
b268	941118	42.939	60.935	961116	*No show*					
b270	941127	39.349	69.551	961021	38.827	64.939	694	66	819.8	4.55
b271	941117	43.338	58.448	961115	*No show*					
b272	950604	43.793	58.774	960812	41.956	65.288	435	66	846.6	4.18
b273	941114	44.531	54.004	950707	44.473	56.255	235	83	794.2	4.43
b274	950610	39.786	69.853	960616	39.896	56.881	372	66	920.8	4.35
b275	941118	43.022	60.995	961116	37.526	70.381	729	00	902.0	4.19
b276	941127	39.787	69.869	961126	38.848	69.360	729	00	1048.2	4.13
b277	941118	42.651	60.655	961116	40.483	47.816	729	00	926.6	4.38
b278	950604	43.331	58.438	970603	*No show*					
b279	941122	42.344	63.324	950404	41.572	64.960	133	83	972.0	4.42
					Deep floats					
b252	941126	38.346	68.783	961124	34.662	59.530	728	00	3017.6	2.67
b254	941118	42.490	60.558	961116	34.586	63.485	729	00	3052.8	2.61
b255	941126	38.561	69.013	961124	27.091	74.319	728	00	2985.6	2.51
b256	950604	43.331	58.438	961021	36.482	71.709	505	83	3007.7	2.75
b257	950611	38.538	68.954	970609	41.326	54.051	728	00	3041.1	2.63
b258	941121	41.386	62.542	961117	35.419	56.896	727	00	3127.4	2.66
b259	941113	43.745	54.646	961108	35.525	71.505	725	00	2992.8	2.71
b260	941117	43.338	58.447	960328	38.161	68.807	497	83	2998.4	2.70
b261	941121	41.733	62.829	961117	*No show*					
b262	941113	43.291	55.082	961108	27.225	75.848	726	00	3585.0	2.48
b264	941116	42.933	58.065	961115	36.734	64.953	729	00	3000.8	2.75
b265	941118	42.385	60.502	961116	38.038	53.185	728	00	2998.0	2.66
b269	941118	42.269	60.407	960904	40.167	52.503	656	80	2989.0	2.73
b280	950603	43.031	58.142	970602	20.751	68.499	729	00	2998.9	2.76
b281	941121	41.398	62.543	950709	34.493	74.037	230	83	3338.8	2.43

launched farther offshore, mostly between the 3500 and 4000 m isobaths (Fig. 2b). The 3000-dbar target pressure for the deep floats was chosen to be several hundred meters above the peak tracer values, which are usually found near the seafloor, in order to avoid float grounding.

The floats were tracked using an array of six sound sources moored in the northwestern North Atlantic. One of these was deployed in 1993 by K. Leaman (University of Miami) for a different experiment (Leaman and Vertes 1996), and was useful in extending the tracking area southward from Cape Hatteras. The other five sources were deployed specifically for BOUNCE. Details regarding the sound sources and float data processing can be found in Hunt and Bower (1998).

b. Float performance

Eighteen of the 26 floats that surfaced completed (or nearly completed) their full 2-yr mission (7 shallow and 11 deep, Table 1), while 8 floats surfaced prematurely at various times (5 shallow and 3 deep, Fig. 3). Details are described in Hunt and Bower (1998), but it is worth mentioning here that the most common (6 floats: 3 shallow and 3 deep) reason for the premature end of a float mission was the loss of the ballast weight. In nearly every case, this was correlated to the float grounding and/or dragging along the seafloor as a result of strong cross-slope flow, possibly associated with topographic Rossby wave activity (see next section). Floats that surfaced prematurely still transmitted the data collected up to that point.

The average density at the initial pressure of the shallow floats, calculated from the CTD data at each float launch site, was 27.737, or 0.007 denser than the target density, 27.73. This corresponds to a pressure offset of only about 30–60 dbar too deep and is within the accuracy of the ballasting procedure. Two of the 14 deep floats were ballasted for pressures deeper than the 3000-dbar target: number 281 was intentionally set for 3320 dbar, and number 262 was mistakenly ballasted for about 3600 dbar. The average difference between the target and actual pressure for the deep floats was 59 dbar too deep, but if number 262 is excluded, the av-

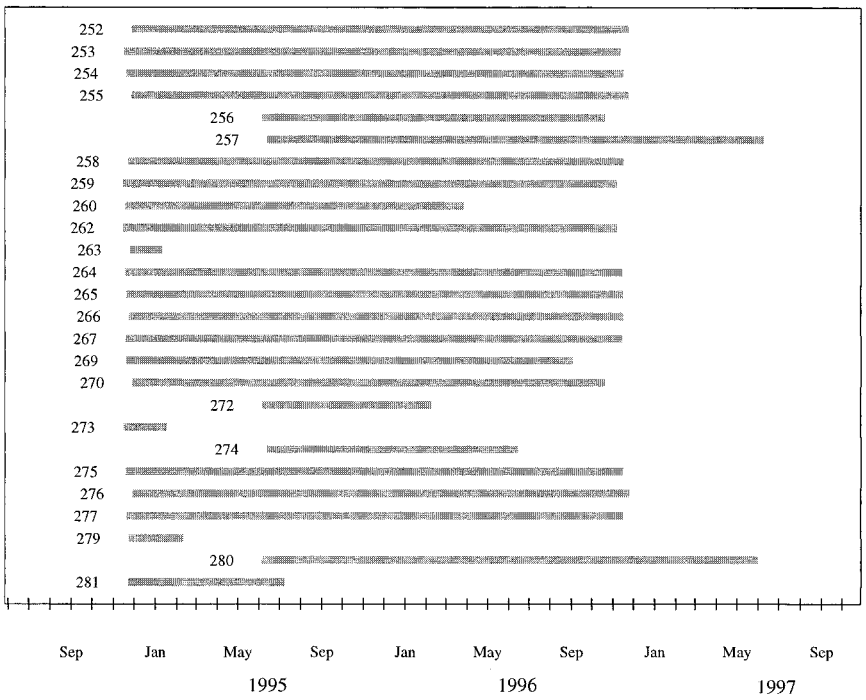

FIG. 3. Schematic chart showing the dates each float was in the water. Float numbers are indicated to the left.

erage difference was only 14 dbar too deep (Hunt and Bower 1998). This is again within the accuracy of the ballasting method.

3. Results

a. Relationship of float deployments to hydrographic properties of DWBC

The objective in this study was to tag the recently ventilated water masses in the DWBC, ULSW, and OW, with floats. In general, this was accomplished successfully. Figure 4 shows the launch locations of the floats relative to the hydrographic property and absolute (synoptic) alongslope velocity distributions for one representative section, BOUNCE I Section 3 (see Fig. 2 for section location). The two shallow floats launched along this section were released at about 900 dbar at initial potential temperatures of 4.3°–4.4°C (Fig. 4a). Initial potential densities were between 27.73 and 27.74 (Fig. 4b). The shallow floats were initially embedded in a relatively large area of high CFC (F-11) concentration (area enclosed by the 1.4 pmol kg^{-1} contour), extending from depth 500 to 2000 m and about 150 km offshore (Fig. 4c). [Within this broad maximum, there was a local maximum exceeding 2.0 pmol kg^{-1} centered at about 1600 m (below the floats). This feature is associated with recently ventilated classical LSW (Molinari et al. 1998; Smethie et al. 2000) which was not targeted by this study.]

Figure 4e shows the initial float positions superimposed on cross-track velocity obtained along Section 3 using the lowered acoustic Doppler current profiler (LADCP) that was attached to the CTD package. The cross-track velocity has a banded structure, with alternating areas of poleward and equatorward velocity about 50 km wide. This is different from the canonical view of the DWBC consisting of an equatorward current banked up against the western boundary, which has been observed farther downstream (Pickart 1992). The banded structure is typical of the absolute velocity sections obtained during BOUNCE I between 55° and 70°W (R. Pickart 1998, personal communication).

The floats launched along this section also revealed spatial (and temporal) variability in the velocity field. Figure 5 depicts the tracks of these floats (2 shallow, 3 deep) immediately after launch. Superimposed on a general equatorward drift of both the shallow and deep tracks are periods of flow reversal, for example at the beginning of the deep float tracks. This is consistent with the launch location of the deep floats in the LADCP section (Fig. 4e), near a transition between poleward and equatorward flow. The cross-slope structure of alongslope velocity is possibly related to the presence of topographic Rossby waves (Pickart 1992). A detailed comparison of the float and LADCP velocities, and an examination of cross-slope and alongslope variability in velocity structure will be the focus of future work. The main point here is that the floats were deployed in high-

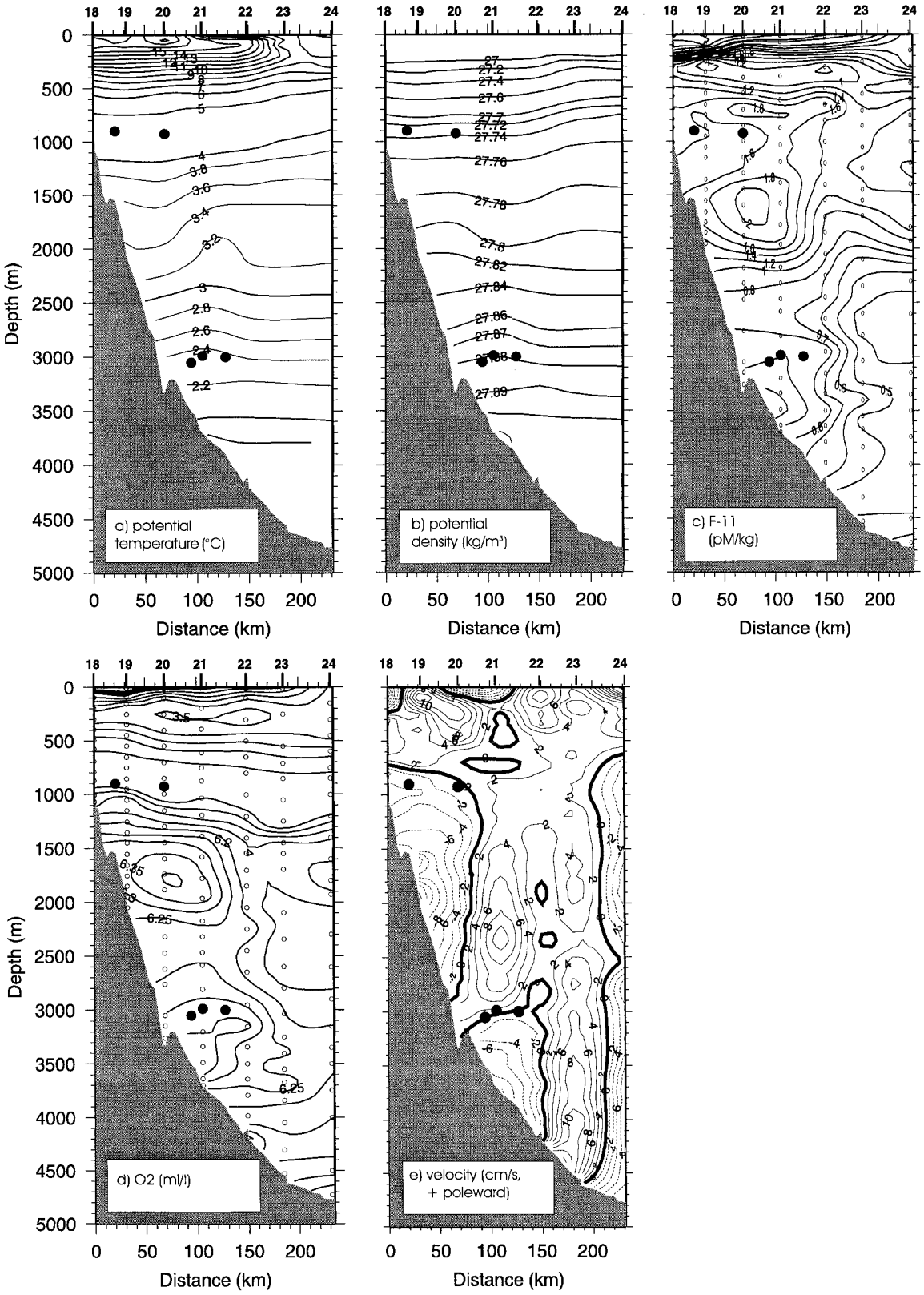

FIG. 4. Hydrographic properties and float launch sites (solid dots) along BOUNCE I Section 3: (a) potential temperature, (b) potential density, (c) CFC (F-11), (d) dissolved oxygen, and (e) absolute alongslope velocity from lowered acoustic Doppler current profiler (LADCP). See Fig. 2 for section location. The continental slope is to the left. The shallow floats were launched at the level of ULSW, and the deep floats were deployed several hundred meters above the bottom in OW.

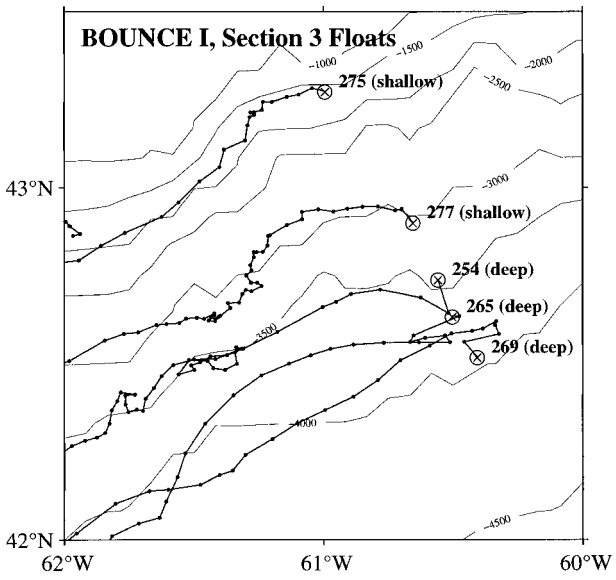

FIG. 5. First part of tracks of five floats deployed along BOUNCE I Section 3, two shallow (275 and 277) and three deep (254, 265, and 269). Dots along tracks indicate daily positions. Launch locations of floats are indicated by circled ×'s. Bathymetric contours are every 500 m.

CFC water that is flowing generally equatorward along the continental slope.

b. Large-scale pathways and spreading rates

1) SHALLOW FLOATS

In Fig. 6a, the complete trajectories of the 12 shallow floats are superimposed on the bathymetry of the western North Atlantic and the meandering envelope of the Gulf Stream. The latter is defined as one standard deviation around the long-term mean Gulf Stream path at the surface, obtained from eight years of Advanced Very High Resolution Radiometer sea surface temperature observations (Lee 1994). The floats that did not ground and lose their weights prematurely (blue tracks; mostly those launched offshore of the 1500-m isobath) generally drifted equatorward along the continental slope (with some cross-slope excursions) to the crossover region, where they were entrained offshore along the path of the Gulf Stream. Only one shallow float was south of the Gulf Stream after two years and its trajectory is shown in Fig. 7a. After being launched between the 2000 and 3000 m isobaths in November 1994, it drifted onshore, then slowly equatorward along the upper slope until June 1995, when it rapidly crossed the continental slope (1). Infrared images of sea surface temperature for this time period show a large warm core ring over the continental slope southwest of the float, which most likely caused the float to be diverted offshore. The float was then briefly entrained into the Gulf Stream (2), indicated by higher eastward speeds and temperatures (not shown), then crossed out of the stream to the north and drifted southwestward over the lower slope from June to October 1995 (3). It was entrained again into the stream near the crossover (4) and advected eastward to about 62°W (5), where it again crossed north of the stream and drifted westward (6). When it was entrained into the stream for the third time, the float started looping cyclonically indicating that it had been caught in a cold core ring, where it remained until it surfaced in November 1996 (7).

The other shallow floats that reached the crossover region behaved similarly in that they were entrained into the Gulf Stream, advected eastward, and crossed out of the stream one or more times to the north. However, except for the float described above, none of them crossed ''permanently'' to the south of the stream in two years. For example, float 270 (Fig. 7b) was launched between the 2000 and 3000 m isobaths near 69.5°W. It drifted steadily equatorward to the crossover region (1), then turned sharply offshore along the path of the Gulf Stream (2). It looped briefly out of the stream to the north, indicated by the cyclonic loops and the cooler temperatures (not shown) (3), then drifted rapidly eastward in the stream to about 55°W (4). Here it decelerated, turned northward, then southwestward, and approximately followed the 4000-m isobath all the way to about 68°W before being entrained into the stream again (5). It crossed north of the stream again (6), drifted slowly westward (7), then surfaced only about 300 km from where it had been launched. This float stayed north of or at the northern edge of the Gulf Stream for its entire 2-yr mission.

The net displacement vectors of the shallow floats (Fig. 6b), clearly show that only one of the seven full-mission floats (blue arrows) (about 15%) ended up well south of the Gulf Stream's meandering envelope after two years. Another full-mission float, number 275, was near the southern edge of the meandering envelope, but all the other floats (including the short-mission floats, red arrows) were either within the Gulf Stream's meandering envelope, or north of it, after two years.

The float data can be used to make direct estimates of both the meridional spreading rate of ULSW and the mean advective rate of ULSW in the DWBC. The former is calculated from the net displacements of the floats, and the results are listed in Table 2. Considering only the seven full-mission floats, the range in mean zonal velocity was -1.6 to $+1.7$ cm s^{-1}, and the overall mean, westward at -0.2 ± 0.4 cm s^{-1}, is not significantly different from zero. The standard error of the mean was calculated assuming (conservatively) that each float is an independent sample. This is justified by the fact that the Lagrangian integral timescale (estimated from the autocorrelation function for the floats) is about 10 days, and floats launched along the same CTD section diverge significantly during the 2-yr mission. Mean meridional velocities were all southward and ranged from -1.2 to -0.1 cm s^{-1}, with a mean of -0.6 ± 0.2 cm s^{-1} southward.

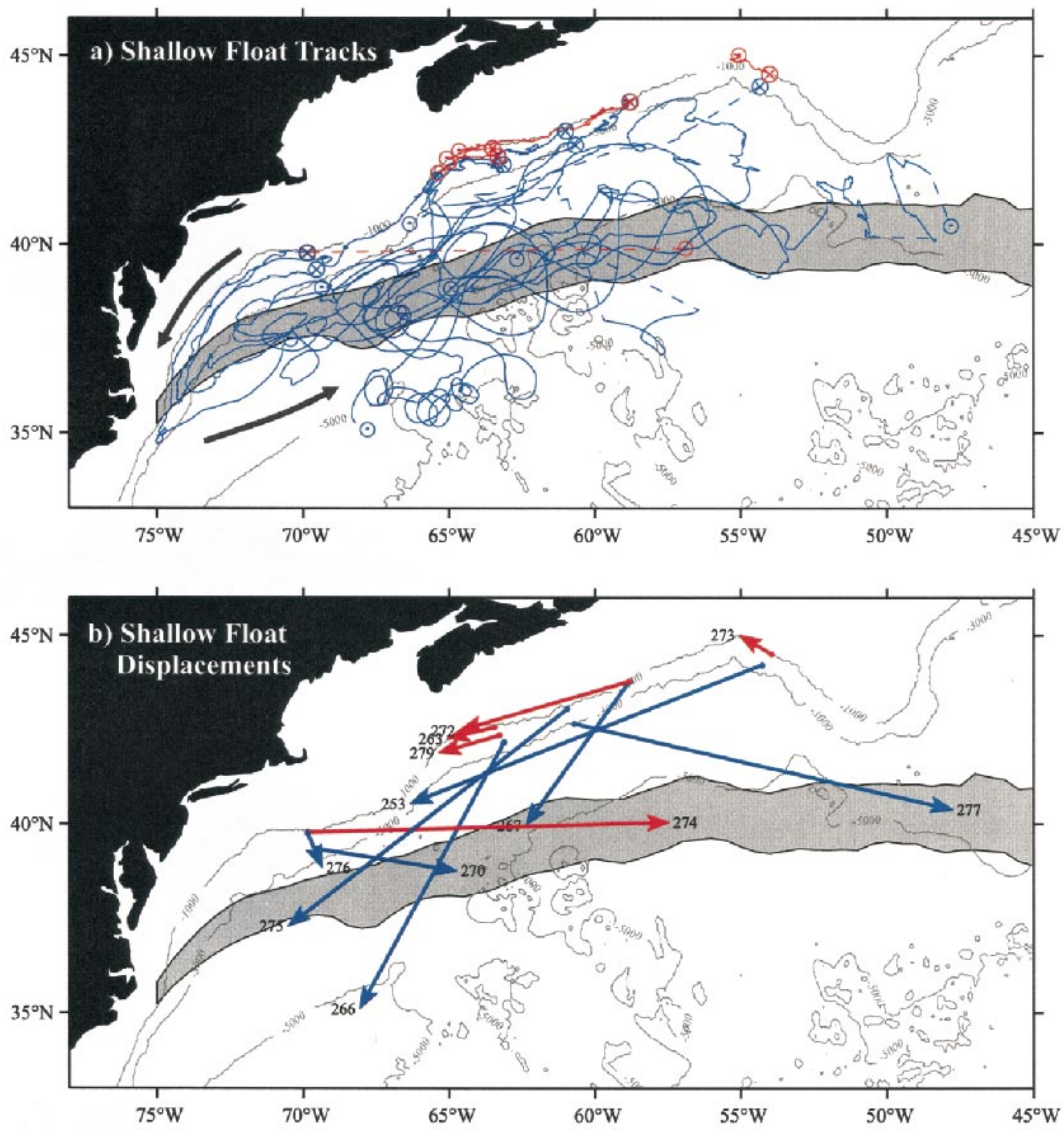

FIG. 6. (a) Twelve shallow float tracks superimposed on the meandering envelope of the Gulf Stream (defined as one standard deviation around the 8-yr mean position of the north wall of the Gulf Stream at the surface). Two-year tracks are in blue, and shorter tracks in red. Launch positions are indicated by circled ×'s, and surface positions by circled dots. Schematic arrows show general direction of float movement. (b) Net displacement vectors of shallow floats. Float numbers are shown near arrowheads. Only one of the 2-yr floats, number 266, was well south of the Gulf Stream's meandering envelope at mission's end. Bathymetric contours are at 1000, 3000, and 5000 m.

To estimate the mean advection rate in the DWBC, we first transformed the daily estimates of float velocity from geographic coordinates to bathymetric coordinates. This was accomplished by estimating a linear bottom slope at each float position from the ETOPO5 digital bathymetric data in a 100 km by 100 km square area around the float position, and rotating the float velocity into along- and across-slope components. The transformed velocities were then plotted as a function of bottom depth and averaged in 500-m bathymetric bins, Fig. 8a. The large error bars are standard deviations in each bin and the small error bars indicate standard errors about the mean, assuming one degree of freedom for every 20 days of observations. Data were not included when a float was either aground or entrained into the Gulf Stream. Both of these situations were identified subjectively; the former by noting when the float pressure was close to the bottom depth and float speed was near zero, and the latter by noting when eastward float speed and temperature were relatively high. The mean alongslope flow is equatorward and significantly different from zero across the entire continental slope. Mean estimates are in the range 2–4 cm s^{-1} toward the equator out to about the 2500-m isobath and somewhat

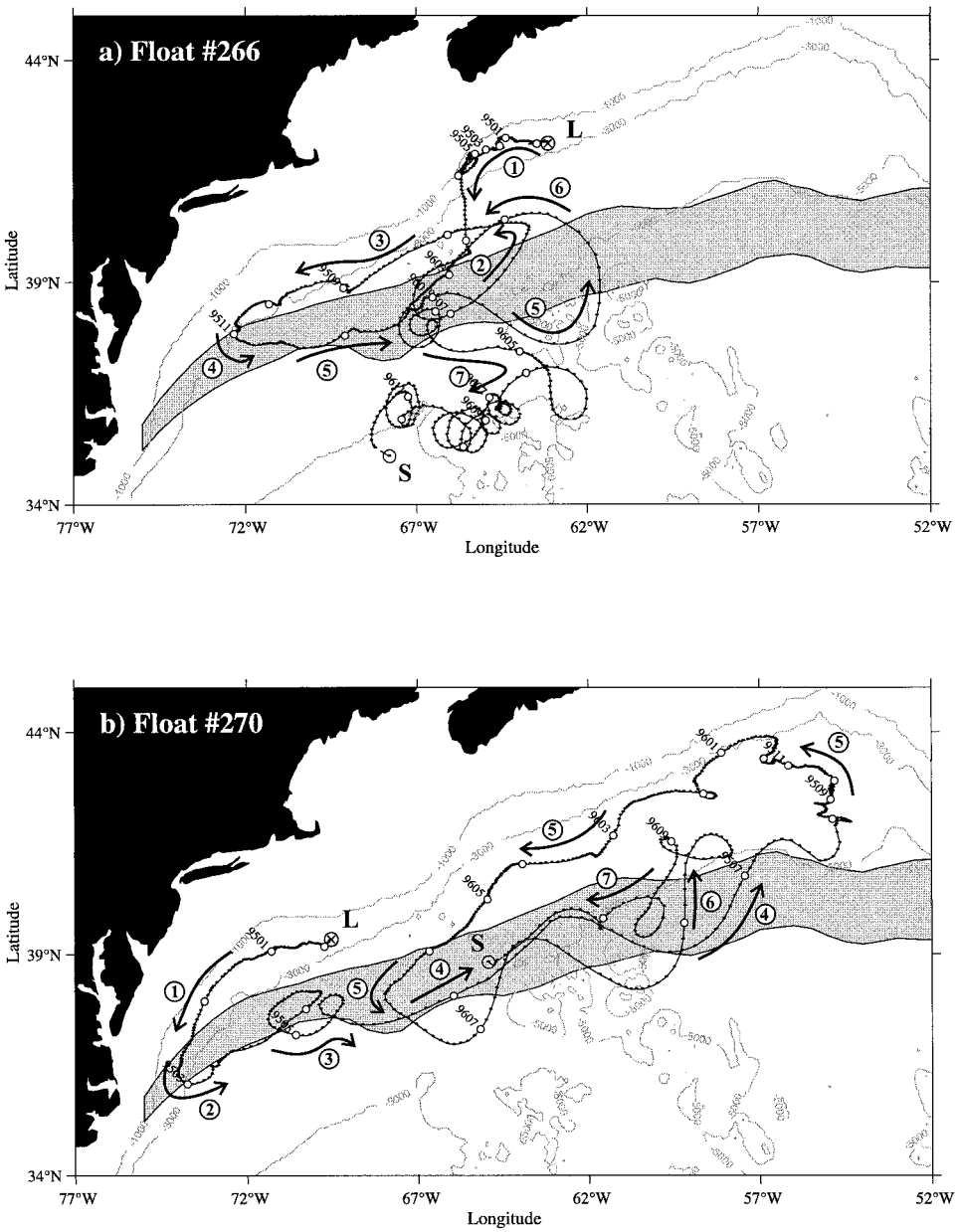

FIG. 7. Representative shallow float tracks: (a) float 266 that was entrained from the upper DWBC into the Gulf Stream and eventually crossed to the south side of the stream in a cold core ring formation event and (b) float 270 that was entrained into the Gulf Stream in the crossover region and then recirculated in the northern recirculation gyre. Circled numbers indicate different parts of the float track, and match description in text. Here L indicates launch position and S, surface position. Small dots show daily positions, and open circles are plotted every month and labeled with the date (yymm) every two months. Bathymetric contours are at 1000, 3000, and 5000 m.

larger, 4–7 cm s^{-1}, farther offshore. Maximum daily values of equatorward alongslope speeds were about 25 cm s^{-1}.

2) DEEP FLOATS

The 14 deep float trajectories, Fig. 9a, closely followed the topography over the slope between 55°W and 72°W. In the crossover region, there is relatively more eddy motion and a bifurcation in float pathways. One branch continues equatorward along the continental slope; the other first follows the mean path of the Gulf Stream to the northeast, then turns southward into the interior. Figure 10 depicts representative deep float tracks for each pathway. Float 280 (Fig. 10b), representing the boundary pathway, was launched over the

TABLE 2. Mean statistics for shallow and deep BOUNCE floats.

Float	Mean Temperature (°C)	Mean Pressure (dbar)	Number of T/P observations	Mean *U* velocity (cm s^{-1})	Mean *V* velocity (cm s^{-1})	Number of days
			Shallow floats			
253	4.2	1065	73	−1.6	−0.6	729
263	4.3	885	49	−3.2	−0.8	48
266	4.8	917	726	−0.6	−1.2	726
267	3.8	1522	729	−0.5	−0.7	729
270	4.5	927	694	0.7	−0.1	694
272	4.1	899	250	−2.2	−0.7	249
273	4.2	829	65	−1.5	1.0	64
274	4.9	1058	366	3.5	0.0	371
275	4.2	1039	729	−1.3	−1.0	729
276	3.8	1515	728	0.1	−0.2	729
277	4.2	1228	729	1.7	−0.4	729
279	4.2	1007	81	−0.7	2.6	80
			Deep floats			
252	3.0	3062	729	1.3	−0.7	728
254	2.8	3073	729	−0.4	−1.4	729
255	2.7	3016	728	−0.8	−2.0	728
256	2.7	3003	504	−2.9	−1.9	503
257	2.9	3081	283	2.0	0.5	728
258	2.9	3161	714	0.8	−1.1	727
259	2.7	3119	721	−2.3	−1.5	725
260	2.9	2998	496	−2.5	−1.5	491
262	2.4	3592	726	−3.0	−2.8	726
264	2.7	3010	728	−0.9	−1.1	729
265	2.9	3026	729	1.0	−0.8	728
269	2.9	3093	657	1.2	−0.4	655
280	2.6	3011	730	−1.6	−3.9	729
281	2.4	3344	229	−5.1	−3.9	230

4000-m isobath near 58°W in June 1995 and more or less followed the slope equatorward for two years, surfacing near 21°N. Float 254 (Fig. 10a), representing the pathway into the interior, was deployed over the 3500-m isobath near 60°W and also initially drifted equatorward along the continental slope (1), but near 71°W it turned eastward (2) and followed the path of the Gulf Stream (3). After briefly crossing out of the stream to the north in April 1996 (4) (deduced from the cyclonic loop), the float track turned southeastward, drifted slowly along the southwestern flank of the New England Seamount Chain, then northwestward along the northeast flank of the Bermuda Rise (5).

Unlike the shallow floats, almost all of the deep floats were south of the Gulf Stream's meandering envelope at mission's end. The displacement vectors (Fig. 9b) show that 9 of the 11 full-mission floats (~80%) had crossed to the south side of the Gulf Stream after two years. About half of these (four floats) were still close to the continental slope—the other half (five floats) were in the ocean interior.

There is only some suggestion of a relationship between where a float ended up and its initial cross-slope position, especially considering the small number of floats. Of the four full-mission deep floats that were deployed farthest inshore (over the 3500-m isobath), two ended up in the interior and two remained close to the boundary. Of the seven full-mission floats released offshore of the 3500-m isobath, five surfaced in the interior and two along the western boundary. So a float deployed over the 3500-m isobath seems to be more likely to remain near the western boundary compared to a float released farther offshore. With so few samples, it is difficult to draw firm conclusions from these observations, but the results are consistent with what one would expect from mixing between the DWBC and the northern recirculation gyre: offshore fluid parcels in the DWBC would be more likely to end up in the recirculation gyre compared to inshore parcels. In Part II, it will be shown that there is a much stronger correlation between cross-slope position of a float *in the crossover region* and whether a float stays along the western boundary or is advected eastward into the interior.

All but one of the deep floats had a net southward displacement (Table 2), and the mean meridional velocity of the 11 full-mission deep floats was -1.4 ± 0.4 cm s^{-1}. This is about twice as large as at the shallower level. The mean zonal velocity however was the same as for ULSW, -0.2 ± 0.5 cm s^{-1}, and not significantly different from zero. The mean advective rate in the deep DWBC was also larger than the inshore part of the shallow DWBC (Fig. 8b). Estimates are about 4.5 cm s^{-1} equatorward out to the 4000-m isobath, then drop to about 2.5 cm s^{-1} farther offshore. The similarity

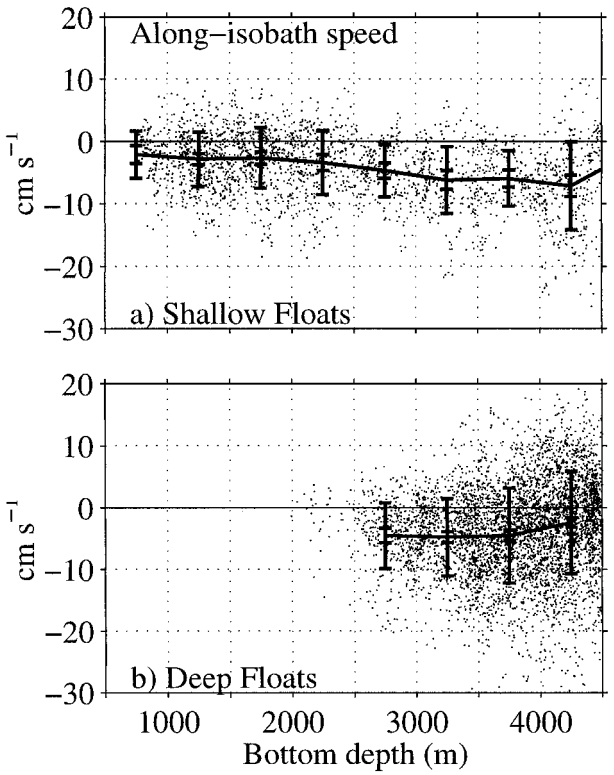

FIG. 8. Along-isobath speed as a function of bottom depth from (a) shallow floats and (b) deep floats. Negative values are equatorward. Small dots indicate daily values, and thick solid line connects the mean values in 500-m bottom depth bins. Large error bars are standard deviation, and small error bars are standard errors about the mean, where the number of degrees of freedom is estimated based on a 10-day integral timescale (see text).

in mean equatorward speeds at the ULSW and OW levels offshore of the 2500-m isobath suggests that the equatorward flow is quite barotropic there, as has been observed in other studies (e.g., Bower and Hogg 1996). All the deep float data were used to make these estimates since eastward flow at 3000 dbar is not necessarily indicative of the Gulf Stream.

4. Discussion

a. Spreading rates of ULSW and OW

The mean meridional velocities estimated from the floats are remarkably (and probably fortuitously, considering the small number of samples) similar to tracer-derived spreading rates. Smethie (1993) estimated the spreading rate of ULSW to be about 0.8 cm s^{-1} based on CFC-11 : CFC-12 ratio distributions, which compares with 0.6 cm s^{-1} estimated from the shallow float observations. Tracer-derived spreading rates for the OW range from 1 to 2.5 cm s^{-1}, with most being between 1 and 2 cm s^{-1} (Doney and Jenkins 1994). These values bracket the overall estimate obtained from the deep float observations, 1.4 cm s^{-1}. Furthermore, Smethie et al. (2000) found relatively younger water in the Gulf Stream region at the ULSW level (<20 yr) compared to the OW level (>20 yr) based on tracer age maps generated from CFC-11 : CFC-12 ratios. This is consistent with the float results: floats at the ULSW level were all entrained into the Gulf Stream, while many of the OW floats crossed under the Gulf Stream and continued equatorward along the western boundary. Leaman and Vertes (1996) obtained a slightly higher southward spreading rate for these water masses farther south, 1.97 $\pm$ 0.0.19 cm s^{-1}, based on the tracks of 23 floats launched in the DWBC near 26.5°N between 1000 and 3000 m. This probably reflects the generally higher velocities of the DWBC core in this region, ~20 cm s^{-1}.

The mean advective rates in the DWBC at the ULSW and OW levels derived from the BOUNCE float observations, 2–4 cm s^{-1} and 4–5 cm s^{-1}, respectively, are higher than the meridional spreading rates by a factor of 3 or more, reflecting that fluid parcels spend significant amounts of time in the interior. The mean DWBC velocities agree well with previous direct observations of the mean flow in the same region. A composite section of absolute alongslope geostrophic velocities at 55°W indicates equatorward speeds of about 2–3 cm s^{-1} at the ULSW level, with very little cross-slope variation (Pickart and Smethie 1998). Johns et al. (1995) produced a composite section of mean westward velocity from current meter observations near 68°W. Mean speeds at 1000 m were westward at 3–4 cm s^{-1} inshore of the 2500-m isobath and increased to almost 6 cm s^{-1} westward over the 4000-m isobath. The offshore values agree very well with those shown in Fig. 8a. The higher speeds reported by Johns et al. inshore of the 2500-m isobath probably result from local acceleration caused by the convergence of the isobaths of the upper slope near 68°W (Fig. 2). Note that there is no evidence of a boundary-intensified jet at the ULSW level in the float (or other) observations: rather, mean equatorward speed increases with offshore distance.

The mean advective rate at the OW level is at the lower limit of the 5–10 cm s^{-1} range, which has been typically reported based on current meter observations (Doney and Jenkins 1994). This is probably because the velocity structure in the deep DWBC is characterized by a slightly bottom-intensified jet, and the floats were drifting several hundred meters above the bottom (e.g., PS93). The mean values in Fig. 8b agree very well with mean westward speeds reported by Johns et al. (1995), 4–5 cm s^{-1} at 3000 m inshore of the 4000-m isobath and decreasing sharply offshore of that isobath. The mean equatorward speed at the OW level obtained from the composite-referenced geostrophic sections at 55°W, ~5 cm s^{-1} (Pickart and Smethie 1998) also agrees well with the float observations.

The float observations also reveal a ''fast track'' for the spreading of OW in the DWBC. Float 280 (Fig. 10b) was launched in the DWBC near 43°N, 58°W in June 1995 and, two years later, it surfaced near 21°N,

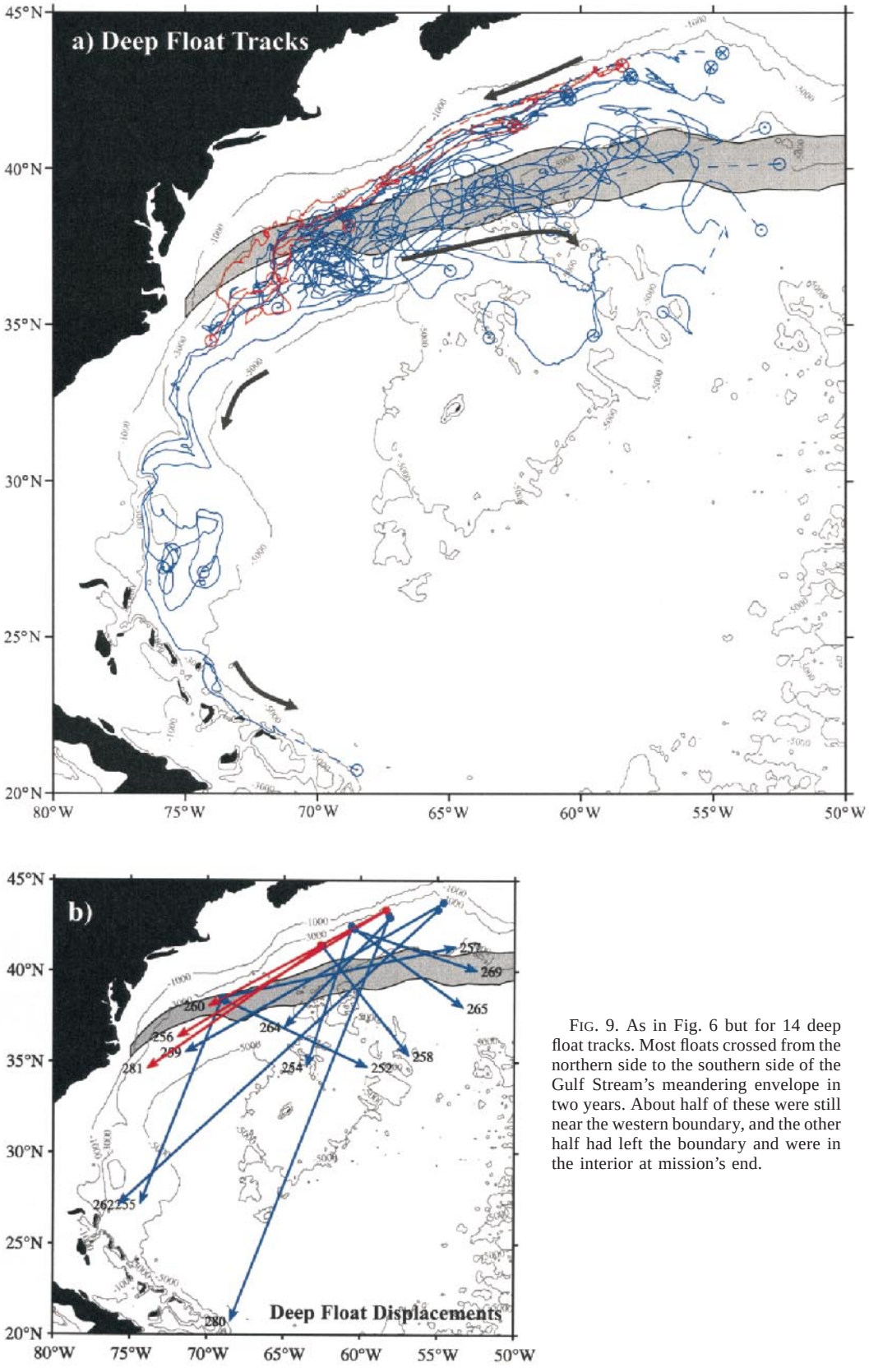

FIG. 9. As in Fig. 6 but for 14 deep float tracks. Most floats crossed from the northern side to the southern side of the Gulf Stream's meandering envelope in two years. About half of these were still near the western boundary, and the other half had left the boundary and were in the interior at mission's end.

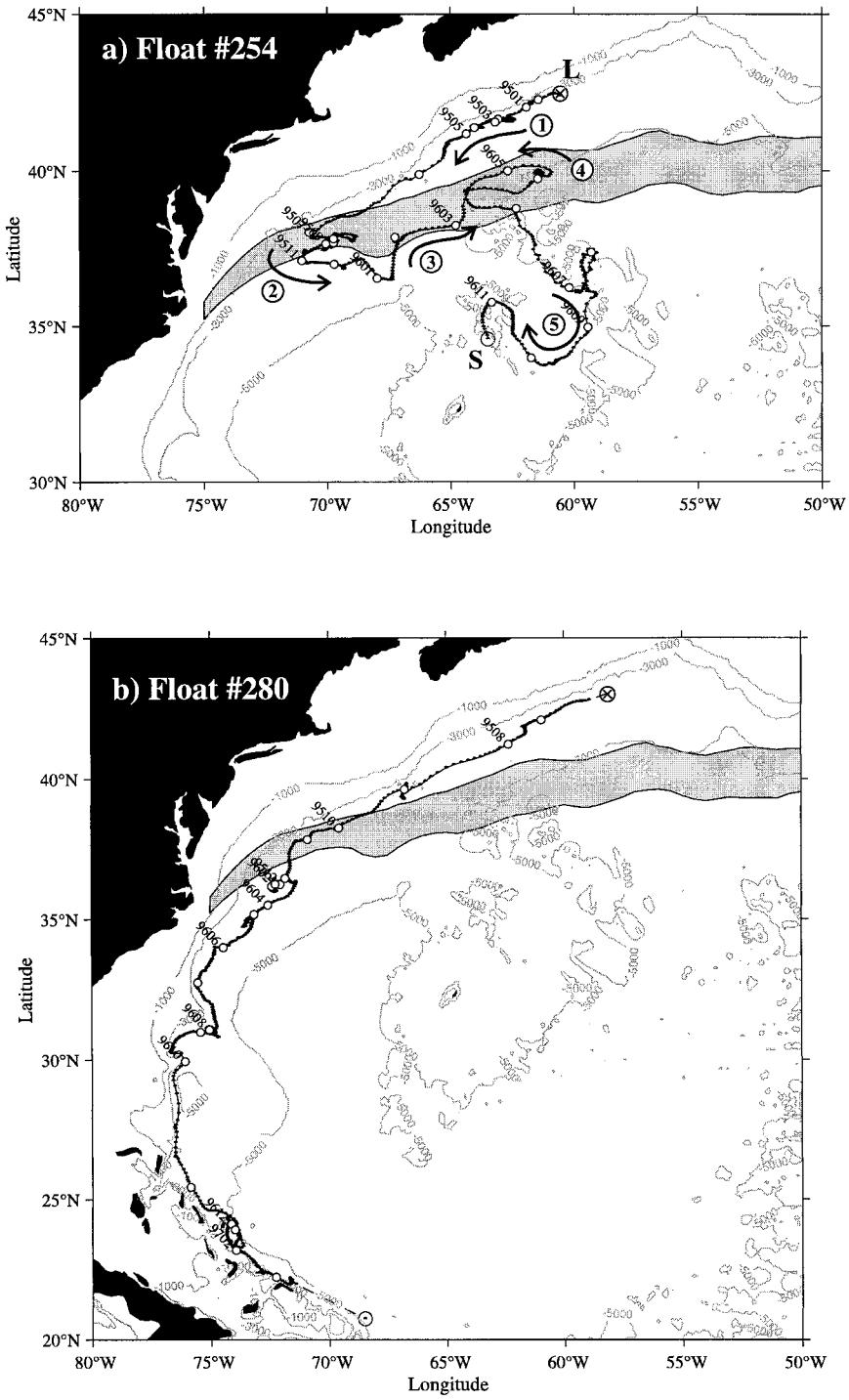

FIG. 10. Representative deep float tracks: (a) float 254, which first drifted southwestward in the DWBC, then eastward along the Gulf Stream path, and eventually southward into the interior; (b) float 280, which drifted continuously equatorward along the western boundary in the DWBC, from 43° to 21°N, in two yrs. Other annotations are as in Fig. 7.

68°W. It drifted more or less directly equatorward, slowing down temporarily in the vicinity of the crossover, then continuing around the Blake Bahama Outer Ridge. Near 24°N, the float made a loop south of the San Salvador Spur, like other floats that have drifted past the spur (Leaman and Vertes 1996), then continued drifting southward along the boundary until it surfaced near 21°N. Thus this float drifted completely through the subtropics in two years. It traveled a total distance along the boundary of 3908 km (using a smoothed version of the 3000-m isobath to estimate along-boundary distance), and the mean along-boundary speed was 6.1 cm s^{-1}. This is about three or more times faster than tracer-derived velocities at the OW level. Molinari et al. (1998) illustrated a similar ''fast track'' based on the arrival at 26°N of classical LSW 8–10 years after formation in the Labrador Sea. Float 280 drifted about half the distance from the Labrador Sea to 26°N in about two years, which implies a total transit time from the Labrador Sea of about four years (extrapolating the mean float speed). This is at least twice as fast as Molinari et al.'s estimate for LSW. The float tracks point to the offshore deflection of intermediate waters at the Gulf Stream–DWBC crossover as a likely explanation for the slower equatorward progression of LSW.

b. Large-scale pathways of ULSW and OW

The shallow floats revealed that fluid parcels in the upper DWBC generally follow the continental slope equatorward between the Grand Banks and Cape Hatteras. There is evidence, however, that warm core rings over the slope can divert ULSW offshore and into the Gulf Stream (Fig. 7a). All of the shallow floats that reached the Gulf Stream–DWBC crossover region were entrained into the Gulf Stream and carried eastward. These observations are consistent with the conclusions of PS93 based on tracer and velocity fields in the crossover region, namely that much of the ULSW in the DWBC is completely entrained into the Gulf Stream at the crossover.

Although the number of samples is small, the shallow float tracks extend the observations of PS93 and provide some insight into the pathways of the ULSW after being entrained into the stream. The most striking characteristic of the shallow float tracks is the rapid eastward advection in the Gulf Stream and the recirculation to the north of the stream. This directly reveals the ventilation of the Gulf Stream and northern recirculation gyre at intermediate depths due to the entrainment at the crossover. The general confinement of the shallow floats to the stream and north of the stream is probably related to the large-scale potential vorticity distribution at this level. Figure 11 shows this distribution on the 27.73 density surface (center of the upper CFC maximum), estimated from climatology of the North Atlantic (Lozier et al. 1995; Curry 1996). Potential vorticity is approximated here by

$$\frac{f}{\rho_o}\frac{\partial \rho}{\partial z}$$

since the relative vorticity is insignificant compared to f at this level. The 27.73 density surface slopes down from about 800 dbar north of the Gulf Stream to 1600 dbar south of the stream. Potential vorticity generally decreases northward, reflecting the weaker stratification of the water north of the Gulf Stream (closer to the convective source). There is a potential vorticity gradient aligned with the mean Gulf Stream path (thick dashed line) across the entire domain. The representative float tracks superimposed on the potential vorticity field (as well as the other shallow floats, Fig. 6a) appear to be generally confined to the region of lower potential vorticity north of the Gulf Stream. This is particularly evident in the crossover region (boxed area), where the floats turn offshore and follow the mean potential vorticity gradient. The notable exception of course is the float that crossed the Gulf Stream in a cold core ring formation event (the rapidly looping track of float 266 in Fig. 11).

Other than ring formation, the shallow floats did not reveal the entrainment of ULSW into the Worthington gyre south of the Gulf Stream, as has been suggested from hydrographic observations and modeling results (PS93; Johns et al. 1997; Spall 1996). In Part II, we will show that the floats do provide some suggestion of a cross-stream mixing mechanism caused by the time-dependent Gulf Stream meandering, even though none of the shallow floats permanently crossed the Gulf Stream via this mechanism. From the float results, we can conclude that the typical residence time for a fluid parcel at the ULSW level north of the Gulf Stream is at least two years. This is not inconsistent with the tracer age map at this level generated by Smethie et al. (2000), which indicates a residence time in the northern recirculation gyre of at least several years.

Like the shallow floats, the deep floats generally followed the continental slope equatorward between the Grand Banks and Cape Hatteras (see Fig. 9a). In the crossover region, a clear bifurcation in pathways was observed, with one branch continuing equatorward near the western boundary and the other turning offshore into the interior. Almost all of the deep floats that followed the offshore pathway eventually turned southward and surfaced south of the Gulf Stream in the subtropical gyre. This pattern is consistent with the deep potential vorticity distribution, Fig. 12. Here we have approximated the potential vorticity by the layer potential vorticity, f/H, where H is the thickness of the deep layer bounded above by the main pycnocline and below by the seafloor. This representation of the lower water column by a single layer is justified based on the relatively weak vertical shear observed below the pycnocline in this region (see Part II). To calculate f/H, ETOPO5 digital bathymetric data were smoothed with a 100-km square box car filter (thin contour lines in Fig. 12). The

filter width was chosen based on an estimate of the internal Rossby radius for the water column below the pycnocline. The pycnocline was approximated as an interface that is flat and shallow north of the Gulf Stream, slopes downward by 750 m over 100 km across the stream, and is flat and deep south of the stream. This first-order representation of the shape of the synoptic pycnocline is supported by climatological hydrographic data, although the slope of the climatological mean pycnocline is weaker than that of the synoptic pycnocline (see Part II). This is due to meandering of the Gulf Stream, which smears out the synoptic structure in the mean. A synoptic model of pycnocline depth was used here in order to simulate the instantaneous pycnocline depth, and thus to give a more realistic picture of potential vorticity encountered by the floats. Hogg and Stommel (1985) generated a similar picture, but they focused on the closed f/H contours north of the Gulf Stream associated with the northern recirculation gyre. Here we consider the effect of the sloping pycnocline associated with the Gulf Stream on the deep f/H distribution over a larger area.

Referring to Fig. 12, it can be seen that the layer potential vorticity distribution (color shading) north and south of the Gulf Stream is dominated by the bottom slope, modified slightly by the planetary vorticity gradient. Clearly visible are the closed potential vorticity contours north of the stream between about 63°W and 52°W, identified by Hogg and Stommel (1985). In the crossover region, the bottom slope over the lower continental slope decreases, and this combined with the sloping pycnocline associated with the Gulf Stream creates a weaker potential vorticity gradient and a ''bulge'' in the f/H contours (also observed by PS93). The presence of the Gulf Stream also results in a ridge of higher potential vorticity extending eastward from the continental slope at about 37°N. This ridge is also apparent in the distribution of gradient potential vorticity

$$\frac{f}{\rho_o}\frac{\partial \rho}{\partial z}$$

on the $\sigma_3 = 41.50$ surface determined from historical hydrographic data (not shown), which is near the center of the OW (PS93).

Superimposed on the potential vorticity field are the tracks of three representative deep floats, 280 and 262 illustrating the branch along the western boundary and 254 depicting the branch that turns offshore into the interior (floats 280 and 254 are shown in more detail in Fig. 10). There is a striking resemblance between these float tracks (as well as all the deep float tracks, Fig. 9a) and the potential vorticity distribution. Northeast of the crossover region, where the potential vorticity gradient over the continental slope is relatively strong, the floats closely followed the slope equatorward. The representative floats were between the 3500 and 4000 m isobaths just before entering the crossover region (near 67°–68°W). In the crossover region, the floats were all displaced offshore, as are the potential vorticity contours. PS93 observed similar behavior in *inferred* fluid parcel trajectories. Floats 254 and 262 exhibited enhanced eddy motion in the region of weaker potential vorticity gradient in the crossover. Float 280 and 262 exited the crossover region toward the south along the continental slope, while float 254 drifted eastward. Note that the tracks of 262 and 254 diverge just where the ridge of higher f/H extends eastward from the continental slope, near 37°N, 68°W. The eastward-drifting float turned southward at the New England Seamount Chain, following the ridge of higher potential vorticity.

The deep fluid parcel pathways revealed by the floats differ from those obtained by Spall (1996) in a three-layer regional primitive equation model. The characteristics of the upper, intermediate, and deep layers in this model were chosen to simulate the Gulf Stream, ULSW, and OW flow fields, respectively. In his deep (OW) layer, Spall did not observe a bifurcation in the mean flow pathways in the crossover region, as we have seen in the float tracks: rather, the equatorward mean flow along the western boundary in the deep layer is diverted just slightly offshore at the crossover and thereafter turns back onshore and continues southward. We believe this pattern is due to the presence of an intermediate layer that largely shields the deep layer from the influence of the sloping interface between the upper and intermediate layers (Spall 1996). Thus potential vorticity in the deep layer is determined mostly by the bottom slope (and f), and fluid parcels in this layer closely follow the topography. Interestingly, Spall *did* obtain a bifurcation in the DWBC pathways in the crossover region in the *intermediate* layer. This layer ''feels'' both the depth changes of the interface with the upper layer and changes in bottom depth (the latter because the lower interface is to a first approximation parallel to the topography; M. Spall 1998, personal communication). This leads to the DWBC flow in the intermediate layer being diverted about 200 km offshore, then splitting into two branches, one continuing southward and the other turning eastward into the interior, very similar to what was observed with the deep floats. The mean potential vorticity distribution in the intermediate layer shows an offshore deflection of potential vorticity contours in the crossover region, similar to the layer potential vorticity field in Fig. 12. The ridge of high potential vorticity extending eastward from the western boundary in Fig. 12 is not apparent in the model: it is eroded quickly by eddy mixing. From this analysis, we conclude that the DWBC fluid parcel pathways at 3000 dbar are strongly influenced by the slope of the main pycnocline as well as the bottom slope, and future modeling efforts should be aimed at including these influences on the deep flow. In Part II, we will show that a two-layer representation of the crossover region is useful in explaining many of the details of the fluid parcel pathways.

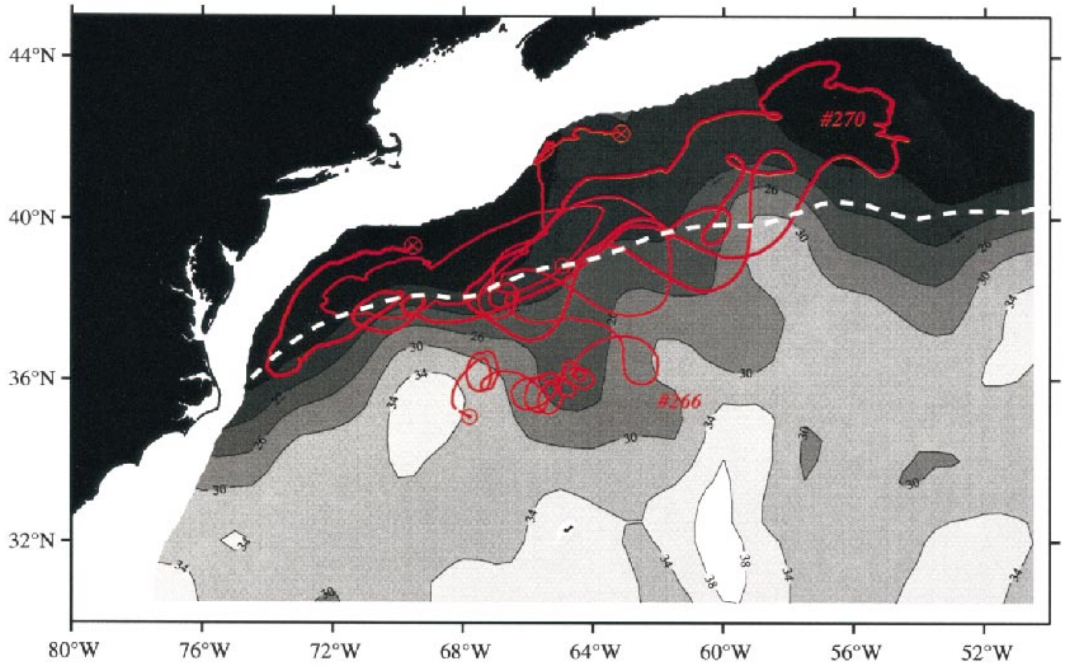

FIG. 11. Mean potential vorticity on the $\sigma_0 = 27.73$ density surface, which is near the center of the CFC maximum associated with ULSW (units are 10^{-12} m^{-1} s^{-1}). The tracks of two representative shallow floats (see individual tracks in Fig. 7) are superimposed in red. Potential vorticity was calculated from station profiles in the HydroBase climatology. The profile data were first isopycnally averaged onto a 1° × 1° grid, and potential vorticity was calculated from the average density gradient at each grid point. The resultant field was then smoothed with a 2° square box car filter. The average number of profiles that make up each grid point is 21, with a range of 1 to 719. Data coverage drops off dramatically east and south of about 39°N, 63°W which probably results in the patchy appearance in that region. The average standard deviation is $\pm 14 \times 10^{-12}$ m^{-1} s^{-1}.

5. Summary and conclusions

The tracks of RAFOS floats deployed at the levels of upper Labrador Sea Water (ULSW) and overflow water (OW) in the DWBC between the Grand Banks and Cape Hatteras have provided the first direct measurements of the effective spreading rates of these two water masses at midlatitudes. The mean meridional velocities, southward at 0.6 ± 0.2 cm s^{-1} (ULSW) and 1.4 ± 0.4 cm s^{-1} (OW), agree very well with indirect, tracer-derived estimates of the spreading rates. The mean advective rates along the western boundary, equatorward at 2–3 cm s^{-1} (ULSW) and 4–5 cm s^{-1} (OW), are similar to estimates based on referenced geostrophic velocities and current meter observations. At the OW level, there is some evidence in the float data of a boundary-intensified jet with mean alongslope velocity decreasing offshore. At the ULSW level, there is no evidence of such a feature: rather, mean equatorward velocity *increases* offshore. The floats also showed that there is a ''fast track'' for the advection of OW southward along the boundary: one deep float traveled 3908 km along the boundary (from 43° to 21°N) in two years, with a mean alongslope velocity of about 6 cm s^{-1}. This is about twice as fast as estimates of a fast-track speed for classical Labrador Sea Water, probably reflecting the more direct route of OW along the western boundary.

The shallow float tracks indicate that ULSW in the DWBC can be deflected off the continental slope north of the Gulf Stream by warm core rings over the slope. The floats also revealed that ULSW is entrained into the Gulf Stream at the location where the deeper parts of the DWBC cross under the Gulf Stream, near 36°N, and carried into the ocean interior, especially into the northern recirculation gyre. Except for one shallow float that crossed the Gulf Stream in a cold core ring formation event, the shallow floats were apparently confined to the region of low potential vorticity north of the Gulf Stream. A residence time of more than two years for the ULSW north of the Gulf Stream is inferred from the float displacements.

The deep float tracks revealed a bifurcation in the pathway of fluid parcels in the deep DWBC at the crossover, with one branch continuing equatorward near the western boundary and the other first turning offshore and following the mean path of the Gulf Stream eastward, then turning southward in the interior. The float pathways are strikingly similar to the deep potential vorticity distribution. The float results suggest that the flow at 3000 dbar is strongly influenced by both the slope of the main pycnocline and the seafloor. The shallow and deep float observations point to the crossover region, addressed in Part II of this study, as important

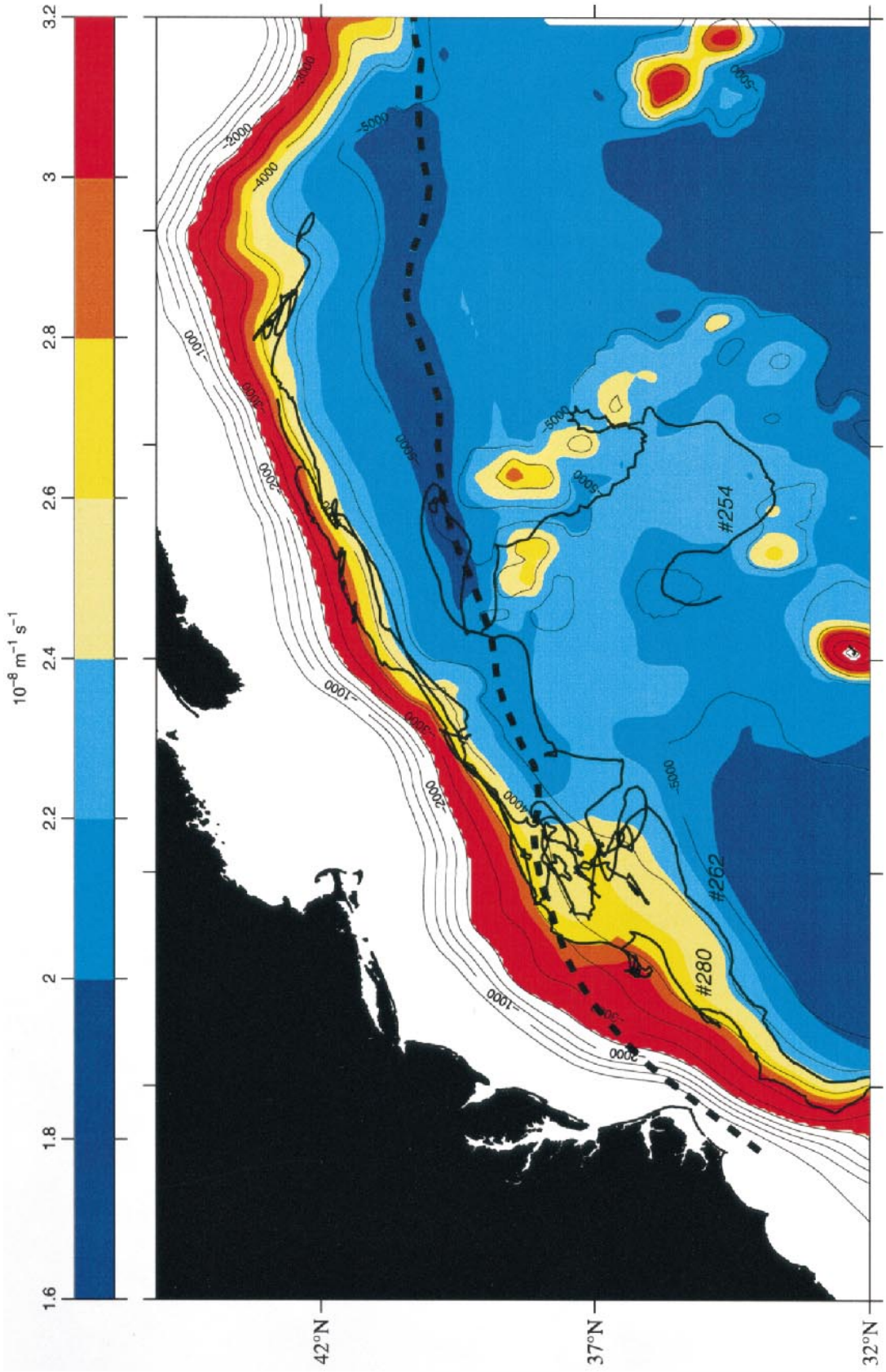

FIG. 12. Layer potential vorticity (f/H, color shading) distribution, where H is the thickness of the deep layer, bounded by the pycnocline and the seafloor (units are 10^{-8} m^{-1} s^{-1}). The pycnocline depth is taken to be flat north of the mean path of the Gulf Stream (thick dashed line), slopes down 750 m over 100 km south of the mean path, and is flat south of the stream. Three representative float tracks are superimposed, illustrating the bifurcation in fluid parcel pathways in the crossover region. The tracks of two of these are also shown in Fig. 10. Smoothed bathymetric contours are indicated by thin lines every 500 m.

in the spreading of recently ventilated water masses that are transported by the DWBC.

Acknowledgments. The authors wish to thank the captains and crews of the R/V *Endeavor*, R/V *Oceanus*, and R/V *Weatherbird II* for their help in the deployment of the sound sources and collection of the observations. J. Valdes, B. Guest, and R. Tavares of the WHOI Float Operations Group are also gratefully acknowledged for their patience and skill in the preparation of the instruments. M. Mensel, then of IFREMER, kindly provided us with his float data processing software and answered many questions. A sound source deployed by K. Leaman of the University of Miami was useful in extending the tracking range of the floats. R. Pickart and D. Torres kindly provided hydrographic data from the BOUNCE cruises. R. Curry provided valuable guidance in the use of the HydroBase climatology. Helpful discussions with R. Pickart, M. Spall, N. Hogg, and W. Smethie contributed to the development of the ideas presented in this paper. The work was supported under Grant OCE93-01448 from the National Science Foundation to the Woods Hole Oceanographic Institution.

REFERENCES

Bower, A. S., and N. G. Hogg, 1996: Structure of the Gulf Stream and its recirculations at 55°W. *J. Phys. Oceanogr.,* **26,** 1002–1022.

——, and H. D. Hunt, 2000: Lagrangian observations of the deep western boundary current in the North Atlantic Ocean. Part II: The Gulf Stream–deep western boundary current crossover. *J. Phys. Oceanogr.,* **30,** 784–804.

Curry, R. G., 1996: HydroBase: A database of hydrographic stations and tools for climatological analysis. WHOI Tech. Rep. WHOI-96-01, 44 pp. [Available from Woods Hole Oceanographic Institution, Woods Hole, MA 02543.]

Doney, S. C., and W. J. Jenkins, 1994: Ventilation of the deep western boundary current and abyssal western North Atlantic: Estimates from tritium and ^{3}He distributions. *J. Phys. Oceanogr.,* **24,** 638–659.

Fine, R. A., 1995: Tracers, time scales, and the thermohaline circulation: The lower limb in the North Atlantic Ocean. *Rev. Geophys.* **33** (Suppl.—U.S. National Report to International Union of Geodesy and Geophysics 1991), 1353–1365.

——, and R. L. Molinari, 1988: A continuous deep western boundary current between Abaco (26.5°N) and Barbados (13°N). *Deep-Sea Res.,* **35,** 1441–1450.

Hogg, N. G., 1992: On the transport of the Gulf Stream between Cape Hatteras and the Grand Banks. *Deep-Sea Res.,* **39,** 1231–1246.

——, and H. Stommel, 1985: On the relation between the deep circulation and the Gulf Stream. *Deep-Sea Res.,* **32,** 1181–1193.

——, R. S. Pickart, R. M. Hendry, and W. M. Smethie Jr., 1986: The northern recirculation gyre of the Gulf Stream. *Deep-Sea Res.,* **33,** 1139–1165.

Hunt, H. D., and A. S. Bower, 1998: Boundary Current Experiment I & II RAFOS float data report 1994–1997. WHOI Tech. Rep. WHOI-98-06, 106 pp. [Available from Woods Hole Oceanographic Institution, Woods Hole, MA 02543.]

Johns, W. E., T. J. Shay, J. M. Bane, and D. R. Watts, 1995: Gulf Stream structure, transport, and recirculation near 68°W. *J. Geophys. Res.,* **100** (C1), 817–838.

——, R. A. Fine, and R. L. Molinari, 1997: Deep flow along the western boundary south of the Blake Bahama Outer Ridge. *J. Phys. Oceanogr.,* **27,** 2187–2208.

Leaman, K. D., and P. S. Vertes, 1996: Topographic influences on recirculation in the deep western boundary current: Results from RAFOS float trajectories between the Blake–Bahama Outer Ridge and the San Salvador ''Gate.'' *J. Phys. Oceanogr.,* **26,** 941–961.

Lee, T., 1994: Variability of the Gulf Stream path observed from satellite infrared images. Ph.D. thesis, Graduate School of Oceanography, University of Rhode Island, 281 pp. [Available from University of Rhode Island, Kingston, RI 02881.]

Lee, T. N., W. Johns, R. J. Zantopp, and E. R. Fillenbaum, 1996: Moored observations of western boundary current variability and thermohaline circulation at 26.5°N in the subtropical North Atlantic. *J. Phys. Oceanogr.,* **26,** 962–983.

Lozier, M. S., 1995: The climatology of the North Atlantic. *Progress in Oceanography,* Vol. 36, Pergamon, 1–44.

Molinari, R. L., R. A. Fine, W. D. Wilson, R. G. Curry, J. Abell, and M. S. McCartney, 1998: The arrival of recently formed Labrador Sea Water in the Deep Western Boundary Current at 26.5°N. *Geophys. Res. Lett.,* **25,** 2249–2252.

Olson, D. B., H. G. Ostlund, and J. Sarmiento, 1986: The western boundary undercurrent off the Bahamas. *J. Phys. Oceanogr.,* **16,** 233–240.

Pickart, R. S., 1992: Space–time variability of the deep western boundary current oxygen core. *J. Phys. Oceanogr.,* **22,** 1047–1061.

——, and D. R. Watts, 1990: Deep Western Boundary Current variability at Cape Hatteras. *J. Mar. Res.,* **48,** 765–791.

——, and W. M. Smethie Jr., 1993: How does the deep western boundary current cross the Gulf Stream? *J. Phys. Oceanogr.,* **23,** 2602–2616.

——, and ——, 1998: Temporal evolution of the Deep Western Boundary Current where it enters the sub-tropical domain. *Deep-Sea Res.,* **45,** 1053–1083.

——, N. G. Hogg, and W. M. Smethie Jr., 1989: Determining the strength of the deep western boundary current using the chlorofluoromethane ratio. *J. Phys. Oceanogr.,* **19,** 940–951.

——, M. A. Spall, and J. R. N. Lazier, 1997: Mid-depth ventilation in the western boundary current system of the sub-polar gyre. *Deep-Sea Res.,* **44,** 1025–1054.

Rhein, M., 1994: The Deep Western Boundary Current: Tracers and velocities. *Deep-Sea Res.,* **41,** 263–281.

Rossby, H. T., E. R. Levine, and D. N. Connors, 1985: The isopycnal Swallow float—A simple device for tracking water parcels in the ocean. *Progress in Oceanography,* Vol. 14, Pergamon, 511–525.

——, D. Dorson, and J. Fontaine, 1986: The RAFOS System. *J. Atmos. Oceanic Technol.,* **3,** 672–679.

Schmitz, W. S., and M. S. McCartney, 1993: On the North Atlantic circulation. *Rev. Geophys.,* **31,** 29–49.

Smethie, W. M., Jr., 1993: Tracing the thermohaline circulation in the western North Atlantic using chlorofluorocarbons. *Progress in Oceanography,* Vol. 31, Pergamon, 51–99.

——, R. A. Fine, A. Putzka, and E. P. Jones, 2000: Tracing the flow of North Atlantic Deep Water using chlorofluorocarbons. *J. Geophys. Res.,* in press.

Spall, M. A., 1996: Dynamics of the Gulf Stream/deep western boundary current crossover. Part I: Entrainment and recirculation. *J. Phys. Oceanogr.,* **26,** 2152–2168.

Stommel, H., 1957: A survey of ocean current theory. *Deep-Sea Res.,* **4,** 149–184.

——, 1958: The abyssal circulation. Letter to the Editors. *Deep-Sea Res.,* **5,** 80–82.

——, and A. B. Arons, 1960a: On the abyssal circulation of the World Ocean—I. Stationary planetary flow patterns on a sphere. *Deep-Sea Res.,* **6,** 140–154.

——, and ——, 1960b: On the abyssal circulation of the World Ocean—II: An idealized model of the circulation pattern and amplitude in oceanic basins. *Deep-Sea Res.,* **6,** 217–233.

Swallow, J. C., and L. V. Worthington, 1961: An observation of a deep countercurrent in the western North Atlantic. *Deep-Sea Res.*, **8,** 1–19.

Talley, L. D., and M. S. McCartney, 1982: Distribution and circulation of Labrador Sea Water. *J. Phys. Oceanogr.*, **12,** 1189–1205.

Watts, D. R., 1991: Equatorward currents in temperatures 1.8°–6.0°C on the continental slope in the Mid-Atlantic Bight. *Deep Convection and Deep Water Formation in the Ocean,* P. C. Chu and J. C. Gascard, Eds., Elsevier, 183–196.

Weiss, R. F., J. L. Bullister, R. H. Gammon, and M. J. Warner, 1985: Atmospheric chlorofluoromethanes in the deep equatorial Atlantic. *Nature,* **314,** 608–610.